Multiband and Perfect Absorber with Circular Fishnet Metamaterial and its Variations

Yusuf Ozturk [1,2] and A. Egemen Yilmaz [2]

[1] The Scientific and Technological Research Council of Turkey
ULAKBİM, Ankara, 06539, Turkey
yusuf.ozturk@tubitak.gov.tr

[2] Department of Electrical and Electronics Engineering
Ankara University, Ankara, 06830, Turkey
aeyilmaz@eng.ankara.edu.tr

Abstract — In this study, a composite metamaterial unit cell is introduced based on experimentally proven circular fishnet metamaterials (CF-MMs) and its stripped versions to implement an absorber for Ku band microwave regime. The offered MM absorber shows the perfect absorptivity (99.9%), the near perfect absorptivity (96.2%) and the standard absorptivity (58%) over narrow band frequencies 14.28, 14.77 and 15.2 GHz, respectively. We offered a method to create a composite metamaterial unit cell consisting of resonant type metamaterial sub-unit cells that are not suitable for absorber implementations in normal conditions. The physical mechanism behind multi-band resonances in the left-handed medium (LHM) regime is explained in detail by revealing the reverse behavior in the right-handed medium (RHM) regime keeping a single resonance feature, based on cancellation of impinging electric fields and preservation of circulating electric fields around the MM space. A detailed analysis is performed to explore and compare the power losses due to imperfect dielectric and non-ideal conductor.

Index Terms — Absorptivity, dielectric loss, composite multiband metamaterial, metamaterial perfect absorber, Q-factor, surface loss.

I. INTRODUCTION

Metamaterials are artificial materials engineered to gain their properties from design challenges such as shape, geometry, size or orientation rather than from their chemistry or composition. By combining electric and magnetic responses together, metamaterials allow for the explicit design of the effective macroscopic parameters. Practical outcome is a negative refractive index (NRI) or double-negative material (DNM) whose effective electric permittivity (ε_{eff}) and magnetic permeability (μ_{eff}) are negative simultaneously in a certain frequency range [1, 2]. Creating an effective medium with controllable permittivity and permeability makes this metamaterials very interesting for many applications, such as superlenses [3, 4], phase shifters [5], antennas [6, 7], cloaking [8, 9], as well as many other devices which have been designed and studied. For many other applications, a key metamaterial performance would be desirable to minimize the metamaterial losses [10, 11]. On the other hand, absorbers focus on maximizing these losses to avoid all types of scattering electromagnetic fields outward the inclusion. An absorber is a device in which all incident radiations including transmissivity, reflectivity and scattering are absorbed at the desired frequency. Electromagnetic (EM) wave absorbers can be categorized into two types: resonant absorbers and broadband absorbers [12]. Resonant absorbers require the material interacting with the incident radiation in a resonant way at a specific frequency, ω_0 (where the wavelength corresponding to ω_0 defined as $\lambda_0 = 2\pi c/\omega_0$ and c is the speed of light in vacuum). Broadband absorbers generally rely on materials whose properties are non-dispersive and therefore can absorb radiations over a large bandwidth. The absorbers employed in everyday applications based on the Salisbury screen [13] are usually backed by a metallic plate to avoid power transmission on the other side of the absorber. In the Salisbury screen layout, a 377 Ω-resistive sheet is placed a quarter-wavelength apart from the metallic plate, where the tangential component of the electric field has its maximum amplitude. Suitable boundary conditions create a reflected component, when combined with the impinging wave, cancels out the reflection from the screen.

The first metamaterial perfect absorber (MPA) consists of three layers, two metallic layers and a dielectric, and demonstrated a simulated absorptivity of $A \approx 99\%$ at 11.48 GHz [14]. Other examples of resonant absorbers were also proposed lately containing three or more layers of symmetrical coupling structures and exhibiting narrow-band absorptivity [15, 16]. Absorbers

Submitted On: August 1, 2016
Accepted On: October 7, 2016

1054-4887 © ACES

based on the regular split-ring resonators (SSRs) disposed in an array configuration are shown to reach thickness of the order of $\lambda_0/20$ [17]. On the other hand, some of multiband metamaterial absorbers take place as good examples, which are composed of six close rings distributed in two metallic layers separated by FR-4 substrates [18], dipole mode electric resonators coupled by microwave diodes on one side of a dielectric substrate and metallic ground plane on the other side [19], 2×2 array of eSRRs oriented in different directions [20]. Physical explanations for absorbance mechanism include lossy substrates and the destructive interference of EM wave with superposition and counteraction for different components [21], plasmonic perfect absorbance based on a Fabry–Perot cavity bounded by a resonator mirror and metallic film [22], or the weak surface current area to avoid the radiation property deterioration [23].

In this study, we designed a multiband metamaterial absorber based on the circular fishnet metamaterial (CF-MM) structure which is shown double-negative (DNG) properties experimentally and theoretically [24]. The dispersive transmission line parameters explain a complex resonance behavior or loss/gain mechanism for CF-MM [25]. At first glance, CF-MM structure shows resonant type transmission properties and the transmission/ reflection coefficients have mutual-exclusive mode that is an undesirable feature for absorber design. To avoid this obstacle, we designed a novel composite CF-MM cell containing itself and stripped variations together. All sheets are designed to operate at a distinct wavelength, and thus, each sheet is separated by approximately λ/9, producing multiple reflection minima around some center frequency. As a contribution, the main reason for multiband features is explained in physical meaning. Additionally, power losses are calculated for each non-ideal conductor sheets and imperfect dielectric layer, separately.

II. STRUCTURE DESIGN AND FABRICATION

Firstly, circular fishnet metamaterial (CF-MM) operating independent of the incident polarization is designed, fabricated and measured in order to characterize its behavior completely. Polarization independency of the structure is due to its symmetric configuration. A schematic view of unit cell, multilayer and equivalent slab pair forms of CF-MMs are depicted in Fig. 1.

The structure consists of the low-loss Teflon substrate (ε_r=2.16 and loss tangent of tanδ=0.005) with a transparent view and the highlighted metal parts as copper layer. The lower tangent loss value is vital to achieve left-handed resonance behavior, therefore FR-4 like substrates are not suitable to create CF-MM in the same dimensions. The Teflon layer as a substrate and the copper layer has t=1 millimeter and 20 micrometer respectively. The unit cell as shown Fig. 1 (a), has the complementary parameters wherein choosing the dimensions as a_x=a_y=a=14 mm and the radius r=0.25×a result in a fully circular and polarization-independent inclusions. The unit cell is replicated nine times in x and y directions to obtain the whole one-layer CF-MM structure including 10×10 cells. For multilayer deployment of CF-MM's as in Fig. 1 (b), the distance between stacked layers shall be set as a_z=2 mm. The incident EM wave propagates along the z-direction perpendicular to the $\boldsymbol{E}$-field parallel to the y-axis and the $\boldsymbol{H}$-field parallel to the x-axis.

In Fig. 1 (b), 1-Stripped CF-MM inclusion (1S-CFMM) is introduced with two complementary design parameters: the strip width (w=0.5 mm) and the gap width between the strip and the main block of copper layer (g=0.2 mm). Due to simplicity, 2-Stripped (2S-CFMM) and 3-Stripped CF-MMs (3S-CFMM) are not presented as stand-alone graphics, indeed they are shown in the composite unit cell (C-CFMM) in Fig. 1 (c). In fact, there are two alternatives to create a composite metamaterial unit cell: sub-modules are placed on the same plate an example of a single planar cell [20] or cascaded form as depicted in [26]. The first one is not applicable for our design due to touching effect of copper layers resulting in a single material rather than a composite metamaterial.

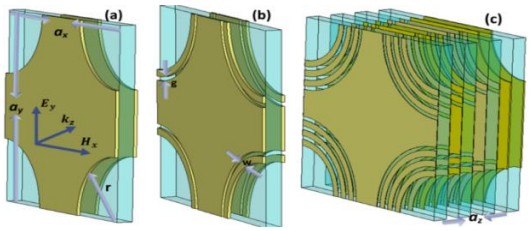

Fig. 1. Schematic representation of CF-MMs as: (a) unit cell, (b) 1-stripped form of the unit cells, and (c) composite CF-MM cell consists of unit cell, 1-stripped, 2-stripped and 3-stripped form of CF-MM cell.

III. EXPERIMENTAL RESULTS AND NUMERICAL CALCULATIONS

First, we investigate the resonance behavior of structure to satisfy the desired operation conditions of DNG medium properties. Due to experimental limitations, the 0-Stripped CF-MM sheet was merely fabricated and measured (Fig. 2). We excite the unit cell displayed in Fig. 1 (a) with a waveguide port and obtain the transmission amplitudes by another waveguide port. The distance between the device under test and the waveguide ports is a_z/2=1 mm. The propagation direction is along +z and electric field vector ($\boldsymbol{E}$) is directed to +y. Moreover, open boundary conditions are employed along the propagation direction (+z and -z). All tangential electric fields in y direction and all tangential magnetic fields in x direction are set to zero to realize electric

boundary conditions and magnetic boundary conditions, respectively. As depicted in Fig. 3 (a), the unit cell has a LHM and RHM resonance centered around 13.8 GHz and 18.5 GHz, respectively. In order to further investigate the properties of CF-MM and its stripped variations, the standard retrieval procedure [27] is applied to extract the effective permittivity and permeability values. The related retrieved effective parameters are shown in Fig. 3 (b). The calculated DNG regions for CF-MM and its variations (1S-CFMM, 2S-CFMM, and 3S-CFMM) are placed at 13.8, 14.2, 14.7, and 15.2 GHz, respectively.

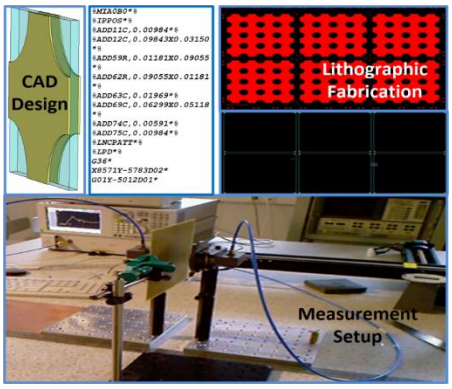

Fig. 2. Schematic representation of the whole process explaining design, sample gerber file, fabrication and measurement of CF-MMs.

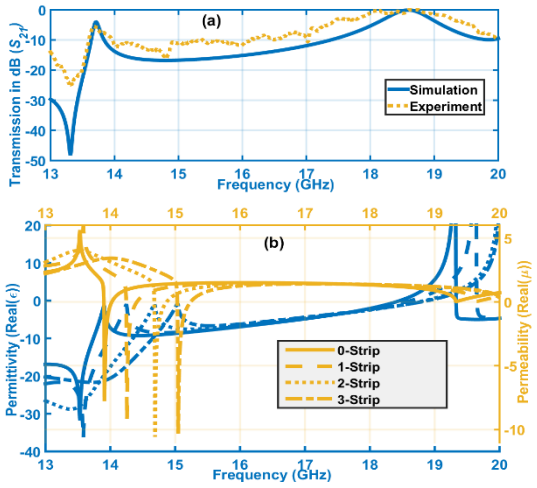

Fig. 3. Numerical and experimental results for $r = 0.25a$: calculated transmission (the blue solid line), measured transmission (the orange dashed) (a), and calculated effective macroscopic parameters (b).

During simulations, the same behaviors of LHM and RHM regimes are obtainable for 1S-CFMM, 2S-CFMM, and 3S-CFMM unit cells except from a frequency-shipping coming from the additional strip capacitance and inductance values. The LHM resonance values in the transmission spectra are calculated 14.22, 14.75, and 15.2 GHz for these inclusions. The phase advance and lag characteristics are also observable in the similar manner. Figure 4 (a) presents the transmission spectra of the composite CF-MM inclusion where S_{11} and S_{21} denote the reflection and transmission coefficients. After this operation, the impedance of the C-CFMM is calculated according to Eq. (1) and compared to the free space impedance:

$$Z(\omega) = \sqrt{\frac{(1+S_{11})^2 - {S_{21}}^2}{(1-S_{11})^2 - {S_{21}}^2}}. \quad (1)$$

The experiments for the CF-MM absorber are performed in free space and at room temperature by using two standard-gain horn antennas. The distance between the horn antennas was kept fixed at 30 cm, away and the absorber under test consisting of 10×10 cells was located at the centeral position. Firstly, a TRL calibration procedure was implemented on the network analyzer in order to eliminate the environmental noises. After the calibration, the transmission spectra have been measured at the same position.

It is necessary to check real and imaginary parts of the retrieved line impedance to control the well-known passive medium requirements. As depicted in Fig. 4 (b), the matching performance of the device reveals the normalized line impedance as 1.5, 1, 0.5, and 0.1 ohms for the resonances 13.8, 14.22, 14.75, and 15.2 GHz, respectively. At around 14.22 GHz, the expected impedance values are easy to achieve for perfect metamaterial absorber applications.

The frequency characteristics of absorption can be calculated by Eq. (2) where A denotes absorber performance. In this equation, S_{21} coefficient must be taken into account under the condition of lacking a backed metallic plate. Accordingly, there are four distinct absorptive peaks belonging to each internal modules with absorption values as 96.2%, 99.99%, 58%, and the negligible one 2.5%. As can be seen from the results in Fig. 4 (c), perfect absorption only occurs with very narrow band at resonant frequency centered at 14.28 GHz, and nearly perfect absorber at 13.82 GHz:

$$A(\omega) = 1 - R(\omega) - T(\omega) = 1 - {S_{11}}^2 - {S_{21}}^2. \quad (2)$$

Obviously, the designed MM absorber has narrow-band absorptivity, and it is possible to achieve perfect absorption in different resonance frequency points by changing the sizes of the structures and dielectric of the substrate materials by supplying sub-wavelength criteria. According to some previous studies [28, 29], the effect is that it acts as a resonant absorber over multiple wavelengths, achieving a broadband response. The bandwidth should increase with each added layer; however, this has the undesirable effect of making the absorber thick and bulky. In our design, the layered unit cells do not play a critical role to change bandwidth of the absorber, clearly.

Power losses inside C-CFMM structure are calculated for each resonance frequency to better

understand the composite unit cell. The results were plotted in Fig. 5 as a bubble graphic. Based on the surface currents created on the each variation of CF-MM cells in the LC resonant mode, the maximum power loss calculations conform with the previous results to a great extent. For 13.82 GHz, the maximum power losses were occurred in the CF-MM module with no-strip. On the other hand, the frequencies of 14.28/14.77/15.2 GHz were correspondent to 1S-CFMM, 2S-CFMM and 3S-CFMM sub-modules as expected.

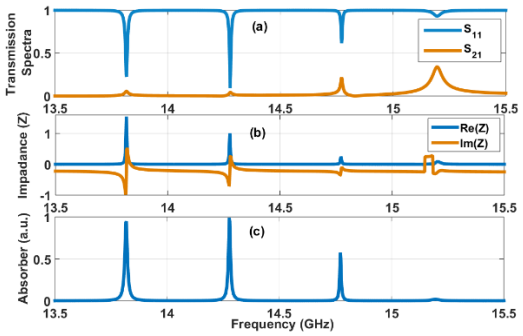

Fig. 4. Calculated transmission/reflection coefficients (a), impedance values (b), and absorbance performance (c) for the C-CFMM unit cell.

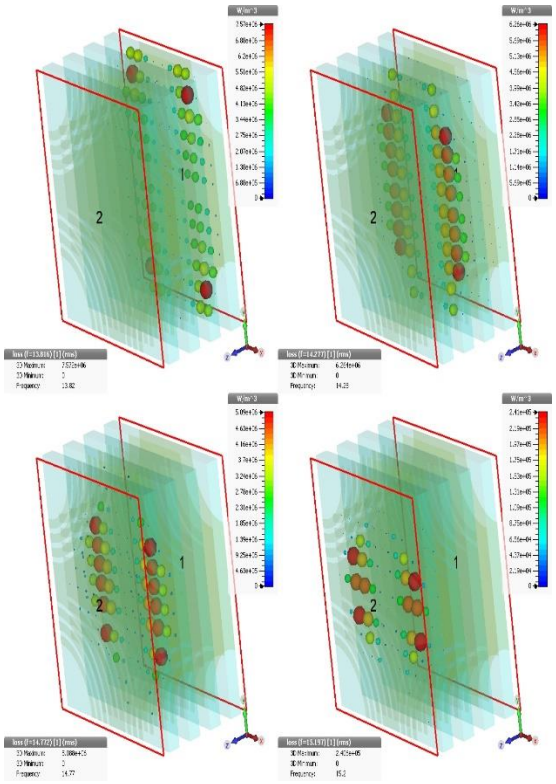

Fig. 5. Power loss density calculations inside the C-CFMM structure for 13.82 GHz (a), 14.28 GHz (b), 14.77 GHz (c), and 15.2 GHz (d).

IV. PHYSICAL EXPLANATIONS

In this section, a detailed physical examination is performed to understand the actual behavior of multiband metamaterial absorbers. First of all, we focus on the question how every sub-module keeps its own behavior like an isolated device. It is easy to observe the omitted fringing electric field intensities in the LHM regime; along the circular sides of CF-MM [24]. As a basic physical explanation, the relationship between the electrical permittivity ε_r and the electric polarization $\boldsymbol{P}$ is defined with the basic formula of $\boldsymbol{D} = \varepsilon_0\boldsymbol{E} + \boldsymbol{P}_e = (1+\chi_e)\varepsilon_0\boldsymbol{E}$. In the situation $\chi_e < -1$, ε_r becomes negative satisfying the homogenization subwavelength conditions. This effect results in that the electric polarization $\boldsymbol{P}$ overcomes the electric flux density term of $\varepsilon_0\boldsymbol{E}$. The same approach can be used in order to analyze the relationship between the effective magnetic susceptibility χ_m and the magnetic flux density $\boldsymbol{B}$ with the second complementary formula $\boldsymbol{B} = \mu_0(\boldsymbol{H} + \boldsymbol{P}_m) = (1+\chi_m)\mu_0\boldsymbol{H}$. This cancellation of the horizontal electric field components produced by circular slots and the corresponding anti-parallelism changes in the surface currents.

On the other hand, the fringing electric fields and the relevant parallel surface currents reshape dispersive nature of multiband absorber. By using a single CF-MM unit cell (shown as blue transparent), electric field components are calculated for LHM (13.8 GHz) and RHM (18.5 GHz) as depicted in Fig. 6, where the numbers "1" and "2" are the waveguide port numbers normal to the surface plane of CF-MM. The distance between the unit cell and the waveguide ports is set to $5xa_z$=10 mm to observe the electric field distributions. The excitation with arbitrary $e^{i\beta r}e^{-i\omega t}$ plane-wave, E-fields are assumed uniformly distributed all over the array according to homogeonization approach. This assumption supplies an averaged space-time distribution of the induced fields with the same $e^{i\beta r}e^{-i\omega t}$ dependence, in which the variables ω and β are independent of each other.

Similar anaysis is performed for causality properties of metamaterial to check Kramers-Kronig relations [30]. The interesting point is that the variables r and β may have corresponding dependency based on Fig. 6. For LHM region, C-CFMM is breaking homogenization approach and each sub-module has own dispersive β characteristics. On the other hand, the same parameters obey homogeonization scheme completely for RHM bands in that conditons there is single RHM resonance different from multiple LHM resonances. Similar composite metamaterial cells can be analyzed with this approach.

Lastly, MPA performance is analyzed here to consider realistic losses in the metals (called as surface loss power and denoted as P_W) and volume losses in the

dielectric substrates (called as volume loss power and denoted as P_D). In the simulations and power loss calculations, the structure has been simulated employing CST Microwave Studio, a full-wave commercial code based on the finite integration technique, with periodic boundary conditions [31]. In order to solve the integral form of Maxwell's equations numerically a finite calculation domain is defined, enclosing the considered application problem. Then, this domain is split up into several small grid cells to create a useful mesh system. Waveguide ports are handled inside the structure, which is quite useful for simulations and physical excitations. The dissipated power on the imperfect dielectric layer strongly depends on the parameters the loss-tangent value taken as $tan\delta = 0.005$ and the electric permittivity taken as $\varepsilon_r = 2.16$ in Eq. (3.1). In normal conditions, the copper layers are assumed to behave as PEC in microwave regimes. During a detailed investigation, the absorbed power due to the nonideal surface losses is calculated with help of the specified conductivity of copper as $\sigma = 5.8x10^7 \mathrm{S/m}$ in Eq. (3.2) [32]:

$$P_D = \pi f tan\delta \varepsilon_0 \varepsilon_r \int |\boldsymbol{E}|^2 \, \partial V, \tag{3.1}$$

$$P_W = \frac{1}{2}\sqrt{\frac{\pi\mu f}{\sigma}} \int |\boldsymbol{H}|^2 \, \partial S. \tag{3.2}$$

The results of the loss power calculations for 14.28 GHz and 14.77 GHz are presented in Table 1, showing very good agreement with the resonances in Fig. 3 and simulations in Fig. 5. According to the table, the surface losses (46.4% and 46.2% for the 1S-CFMM resonance at 14.28 GHz and the 2S-CFMM resonance at 14.77 GHz, respectively) are comparable to the volumetric losses (53.6% and 53.8% for 14.28 GHz and 14.77 GHz, respectively). The maximum surface losses can be seen in 1S-CFMM Copper Surface (33%) and 2S-CFMM Copper Surface (33.5%) for their own LHM resonances as expected. By using this results, Q-factor of device is equal to:

$Q = 2\pi f \times (average\ energy\ stored)/(total\ power\ loss)$.

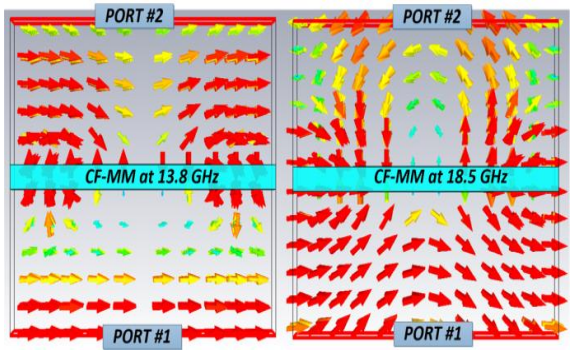

Fig. 6. Top view of the calculated electric field components inside and around the CF-MM structure for 13.8 GHz (left panel) and 18.5 GHz (right panel).

Table 1: Power loss calculation for the C-CFMM inclusion

Loss Region	Loss/W (Peak) at 14.28 GHz	Loss/W (Peak) at 14.77 GHz
CF-MM copper surface	4.8567×10^{-3}	3.9969×10^{-3}
1S-CFMM copper surface	6.1259×10^{-1}	9.3417×10^{-3}
2S-CFMM copper surface	3.5518×10^{-2}	3.4556×10^{-1}
3S-CFMM copper surface	3.6165×10^{-3}	3.4972×10^{-2}
Total surface loss power (P_W)	8.4762×10^{-1}	4.7555×10^{-1}
Total volume loss power (P_D)	9.8087×10^{-1}	5.5461×10^{-1}

V. CONCLUSIONS

In summary, a polarization-independent and narrow-band absorber with triple bands has been successfully designed and tested by using composite circular fishnet metamaterial cells. The resonant inclusions are considered to match the impedance of the absorber to free space and achieve large energy dissipation, minimizing the wave refection and transmitting under the assumption that the scattering is negligible (the roughness of the surface $R \ll \lambda$). The proposed structure does not require a separate resistive sheet or backed metal plate. It is shown that different LHM resonances can occur simultaneously based on cancellation of impinging electric fields. This gives opportunity to design composite unit cells for multiband absorber operations. Power loss calculations result in comparability between metal and dielectric layers of composite circular fishnet metamaterial.

REFERENCES

[1] D. R Smith, W. J. Padilla, D. C. Vier, S. C. Nemat-Nasser, and S. Schultz, "Composite medium with simultaneously negative permeability and permittivity," *Physical Review Letters*, vol. 84, no. 18, pp. 4184, 2000.

[2] R. A. Shelby, D. R. Smith, and S. Schultz, "Experimental verification of a negative index of refraction," *Science*, vol. 292, no. 5514, pp. 77-79, 2001.

[3] K. Aydin, I. Bulu, and E. Ozbay, "Subwavelength resolution with a negative-index metamaterial superlens," *Appl. Phys. Lett.*, vol. 90, no. 25, pp. 254102, 2007.

[4] X. Zhang and L. Zhaowei, "Superlenses to overcome the diffraction limit," *Nat. Mater.*, vol. 7, no. 6, pp. 435-441, 2008.

[5] M. A. Antoniades and G. V. Eleftheriades, "Compact linear lead/lag metamaterial phase shifters for broadband applications," *IEEE Antennas Wirel. Propag. Lett.*, vol. 2, no. 1, pp. 103-106,

2003.

[6] A. Erentok, P. L. Luljak, and R. W. Ziolkowski, "Characterization of a volumetric metamaterial realization of an artificial magnetic conductor for antenna applications," *IEEE Trans. Antennas Propag.*, vol. 53, no. 1, pp. 160-172, 2005.

[7] L. Sungjoon, C. Caloz, and T. Itoh, "Metamaterial-based electronically controlled transmission-line structure as a novel leaky-wave antenna with tunable radiation angle and beamwidth," *IEEE Trans. Microwave Theory Techn.*, vol. 53, no. 1, pp. 161-173, 2005.

[8] W. Cai, U. K. Chettiar, A. V. Kildishev, and V. M. Shalaev, "Optical cloaking with metamaterials," *Nat. Photonics*, vol. 1, no. 4, pp. 224-227, 2007.

[9] A. Alu and N. Engheta, "Plasmonic and metamaterial cloaking: Physical mechanisms and potentials," *J. Opt. A*, vol. 10, no. 9, pp. 093002, 2008.

[10] S. Wuestner, A. Pusch, K. L. Tsakmakidis, J. M. Hamm, and O. Hess, "Overcoming losses with gain in a negative refractive index metamaterial," *Phys. Rev. Lett.*, vol. 105, no. 12, pp. 127401, 2010.

[11] J. Zhou, T. Koschny, and C. M. Soukoulis, "An efficient way to reduce losses of left-handed metamaterials," *Opt. Express*, vol. 16, no. 15, pp. 11147-11152, 2008.

[12] C. M. Watts, X. Liu, and W. J. Padilla, "Metamaterial electromagnetic wave absorbers," *Adv. Mater.*, vol. 24, no. 23, pp. OP98-OP120, 2012.

[13] W. W. Salisbury, "Absorber Body for Electromagnetic Waves," *U.S. Patent* 2599944, June 10, 1952.

[14] N. I. Landy, S. Sajuyigbe, J. J. Mock, D. R. Smith, and W. J. Padilla, "Perfect metamaterial absorber," *Phys. Rev. Lett.*, vol. 100, no. 20, pp. 207402, 2008.

[15] H. Tao, C. M. Bingham, A. C. Strikwerda, D. Pilon, D. Shrekenhamer, N. I. Landy, et al., "Highly flexible wide angle of incidence terahertz metamaterial absorber: Design, fabrication, and characterization," *Phys. Rev. B*, vol. 78, no. 24, 2008.

[16] N. I. Landy, C. M. Bingham, T. Tyler, N. Jokerst, D. R. Smith, and W. J. Padilla, "Design, theory, and measurement of a polarization-insensitive absorber for terahertz imaging," *Phys. Rev. B*, vol. 7, no. 9, 2009.

[17] F. Bilotti, A. Toscano, K. B. Alici, E. Ozbay, and L. Vegni, "Design of miniaturized narrowband absorbers based on resonant-magnetic inclusions," *IEEE Trans. Electromagn. Compatibility*, vol. 53, no. 1, pp. 63-72, 2011.

[18] L. Huang and H. Chen, "Multi-band and polarization insensitive metamaterial absorber," *Prog. Electromagn. Res.*, vol. 113, pp. 103-110, 2011.

[19] B. Zhu, C. Huang, Y. Feng, J. Zhao, and T. Jiang, "Dual band switchable metamaterial electromagnetic absorber," *Prog. Electromagn. Res.*, vol. 24, pp. 121-129, 2010.

[20] M. Li, H. L. Yang, X. W. Hou, Y. Tian, and D. Y. Hou, "Perfect metamaterial absorber with dual bands," *Prog. Electromagn. Res.*, 108, pp. 37-49, 2010.

[21] S. J. Li, X. Y. Cao, J. Gao, T. Liu, Y. J. Zheng, and Z. Zhang, "Analysis and design of three-layer perfect metamaterial-inspired absorber based on double split-serration-rings structure," *IEEE Transactions on Antennas and Propagation*, vol. 63, no. 11, pp. 5155-60, 2015.

[22] K. Bhattarai, Z. Ku, S. Silva, J. Jeon, J. O. Kim, S. J. Lee, A. Urbas, and J. Zhou, "A large-area, mushroom-capped plasmonic perfect absorber: Refractive index sensing and Fabry–Perot cavity mechanism," *Advanced Optical Materials*, vol. 3, no. 12, pp. 1779-1786, 2015.

[23] S. J. Li, J. Gao, X. Y. Cao, Y. Zhao, Z. Zhang, and H. X. Liu, "Loading metamaterial perfect absorber method for in-band radar cross section reduction based on the surface current distribution of array antennas," *IET Microwaves, Antennas & Propagation*, vol. 9, no. 5, pp. 399-406, 2014.

[24] Y. Öztürk, A. E. Yılmaz, E. Çolak, and E. Özbay, "Characterization, slab-pair modeling and phase analysis of circular fishnet metamaterials," *Phot. Nano. Fund. Appl.*, vol. 10, no. 4, pp. 624-631, 2012.

[25] Y. Öztürk, A. E. Yılmaz, and E. Özbay, "Conversion from constitutive parameters to dispersive transmission line parameters for multi-band metamaterials," *Waves in Random and Complex Media*, vol. 26, no. 2, pp. 223-235, 2016.

[26] E. Ekmekci, K. Topalli, T. Akin, and G. Turhan-Sayan, "A tunable multi-band metamaterial design using micro-split SRR structures," *Opt. Express*, vol. 17, no. 18, pp. 16046-16058, 2009.

[27] X. Chen, T. M. Grzegorczyk, B. I. Wu, J. Pacheco, and J. A. Kong, "Robust method to retrieve the constitutive effective parameters of metamaterials," *Phys. Rev. E.*, vol. 70, pp. 016608, 2004.

[28] G. T. Ruck, D. E. Barrick, and W. D. Stuart, *Radar Cross Section Handbook*. vol. 2, New York, Plenum Press, New York, 1970.

[29] B. A. Munk, P. Munk, and J. Pryor, "On designing Jaumann and circuit analog absorbers for oblique angle of incidence," *IEEE Trans. Ant. Prop.*, vol. 55, pp. 186-193, 2007.

[30] A. Alù, "First-principles homogenization theory for periodic metamaterials," *Phys. Rev. B*, vol. 84, no. 7, pp. 075153, 2011.

[31] CST Microwave Studio, ver. 2015, Computer

Simulation Technology, Framingham, MA, 2016.
[32] R. Bansal, *Fundamentals of Engineering Electromagnetics*. CRC Press, pp. 233-235, 2006.

Yusuf Ozturk received his B.Sc., M.Sc. and Ph.D. in Electrical and Electronics Engineering from Ankara University in 1997, 2002, and 2014 respectively. His research interests include image processing, networking technologies, applied electromagnetics, photonics and metamaterials. He is working at the Scientific and Technological Research Council of Turkey (TUBITAK).

Asim Egemen Yilmaz was born in 1975. He received his B.Sc. degrees in Electrical-Electronics Engineering and Mathematics from the Middle East Technical University in 1997. He received his M.Sc. and Ph.D. degrees in Electrical-Electronics Engineering from the same university in 2000 and 2007, respectively. He is currently with the Dept. of Electronics Engineering in Ankara University, where he is an Associate Professor. His research interests include computational electromagnetics, nature-inspired optimization algorithms, knowledge-based systems; more generally software development processes and methodologies.